Poly(*N*-isopropylacrylamide)-Coated Luminescent/Magnetic Silica Microspheres: Preparation, Characterization, and Biomedical Applications

Jia Guo,[†] Wuli Yang,[†] Changchun Wang,*[,†] Jia He,[‡] and Jiyao Chen[‡]

Key Laboratory of Molecular Engineering of Polymers (Minister of Education) and Departments of Macromolecular Science and of Physics, Fudan University, Shanghai, China 200433

Received April 27, 2006. Revised Manuscript Received September 19, 2006

Smart microstructures based on organic/inorganic hybrids were rationally designed to develop applications in the novel interdisciplinary research field "nanobioscience". These multifunctional microspheres, combining several advances of photoluminescence and magnetic and temperature responses into one single entity, have been prepared via three steps. The first step involved magnetite nanoparticles (Fe_3O_4) homogeneously incorporated into silica spheres using the modified Stöber method. Second, metal ions (Cd^{2+}) were utilized to precipitate the differently sized thiol-capped CdTe nanocrystals onto the Fe_3O_4-dotted silica surface with negative charges, and then a thin silica shell was coated on them in favor of formation of a robust platform provided for anticorrosion of quantum dots. Third, the modified silica-coated Fe_3O_4@SiO_2@CdTe microspheres were covered with the outer shell of thermosensitive poly(*N*-isopropylacrylamide) via template polymerization. These hybrid microspheres are desired as carriers for diagnostics, circulating drug-delivery systems, and treating cancer at its earliest stages.

Introduction

Quantum dots (QDs), with unique photophysical properties such as narrow and size-tunable emission spectra, a robust signal intensity, a broad excitation band, and high photochemical stability, have been shown to be ideal for use as fluorophores in multiplexed bioanalysis.[1−5] Nevertheless, almost all applications of nanoparticles require a further derivatization as a prerequisite. Forming composite nanostructures such as biomolecule−QD conjugates,[6] metal−QD nanohybrids,[7] or polymer−QD hybrids[8] is an important step toward applications of these nanomaterials. Recently, substantial progress achieved in several groups has led to a burst of activities in the generation of multicolor optical "bar codes" based on trapping differently sized QDs into microspheres at precisely controlled ratios.[9−13] Using this kind of detection format, a large number of QDs were encapsulated into one protective microsphere. These markers may obtain abundant and intense spectral signatures and be allowed for the real-time study of certain long-lived biological processes.[14] However, so far, integration of multiple QDs with colloidal spheres has still been a challenge for researchers.

To the best of our knowledge, there are three major approaches to the design of multi-QD-entrapped microspheres. The first is to use the polymer spheres as microreactors to produce entrapped QDs in situ.[15] Although the feasibility of the synthesis of QDs in microspheres has been proven, in situ synthesized QDs are generally polydispersed and have low quantum yields. The second route is that prepared QDs are mixed with monomers for polymerization, leading to incorporation of them by chemical multicovalent attachment. However, if QDs preserve the native ligands, the resultant composites usually show bad transparency and poor fluorescence due to aggregation of nanocrystals in matrixes. Thus, polymerizable ligands such as functionalized alkoxysilanes and complexable monomers have been precoated onto the nanocrystal surfaces via ligand exchanges for subsequent polymerization.[16−19] However, as such processes require the modification of the surfaces of QDs, a

* To whom correspondence should be addressed. Fax: 86-21-65640291. Phone: 86-21-65642385. E-mail: ccwang@fudan.edu.cn.

[†] Key Laboratory of Molecular Engineering of Polymers (Minister of Education) and Department of Macromolecular Science.

[‡] Department of Physics.

(1) Bruchez, M. P.; Moronne, M.; Gin, P.; Weiss, S.; Alivisatos, A. P. *Science* **1998**, *281*, 2013.
(2) Chan, W. C. W.; Nie, S. *Science* **1998**, *281*, 2016.
(3) Battersby, B. J.; Bryant, D.; Meutermans, W.; Matthews, D.; Smythe, M. L.; Trau, M. *J. Am. Chem. Soc.* **2000**, *122*, 2138.
(4) Gerion, D.; Parak, W. J.; Williams, S. C.; Zanchet, D.; Micheel, C. M.; Alivisatos, A. P. *J. Am. Chem. Soc.* **2002**, *124*, 7070.
(5) Robelek, R.; Niu, L. F.; Schmid, E. L.; Knoll, W. *Anal. Chem.* **2004**, *76*, 6160.
(6) Riegler, J.; Nick, P.; Kielmann, U.; Nann, T. *J. Nanosci. Nanotechnol.* **2003**, *3*, 380.
(7) Kim, H.; Achermann, M.; Balet, L. P.; Hollingsworth, J. A.; Klimov, V. I. *J. Am. Chem. Soc.* **2005**, *127*, 544.
(8) Kucur, E.; Riegler, J.; Urban, G. A.; Nann, T. *J. Chem. Phys.* **2004**, *120*, 1500.
(9) Han, M.; Gao, X.; Su, J. Z.; Nie, S. *Nat. Biotechnol.* **2001**, *19*, 631.
(10) Gao, X.; Nie, S. *Anal. Chem.* **2004**, *76*, 2406.
(11) Gao, X.; Nie, S. *J. Phys. Chem. B* **2003**, *107*, 11575.
(12) Gaponik, N.; Radtchenko, I. L.; Sukhorukov, G. B.; Weller, H.; Rogach, A. L. *Adv. Mater.* **2002**, *14*, 879.
(13) Kuang, M.; Wang, D.; Bao, H.; Gao, M.; Möhwald, H.; Jiang, M. *Adv. Mater.* **2005**, *17*, 267.
(14) Ho, Y. -P.; Kung, M. C.; Yang, S.; Wang T. -H. *Nano Lett.* **2005**, *5*, 1693.
(15) Zhang, J.; Xu, S.; Kumacheva, E. *J. Am. Chem. Soc.* **2004**, *126*, 7908.
(16) Zhang, H.; Wang, C.; Li, M.; Ji, X.; Zhang, J.; Yang, B. *Chem. Mater.* **2005**, *17*, 4783.
(17) Sherman, R. L., Jr.; Ford, W. T. *Langmuir* **2005**, *21*, 5218.
(18) Nann, T.; Mulvaney, P. *Angew. Chem., Int. Ed.* **2004**, *43*, 5393.
(19) Rogach, A. L.; Nagesha, D.; Ostrander, J. W.; Giersig, M.; Kotov, N. A. *Chem. Mater.* **2000**, *12*, 2676.

10.1021/cm060976w CCC: $33.50
Published on Web 10/27/2006

low photoluminescence (PL) intensity and/or a red shift of the emission peaks were present in the ligand-exchange or polymerization process. Furthermore, it might be difficult to define the QD amount and ratios among different QDs within microspheres for multicolor optical coders. Compared with the first two methods, the third method is based on the multiporous nanostructure from the swelling behaviors of polymer spheres. The preformed QDs have been entrapped within microspheres by different driving forces including hydrophobic interaction,[11] electrostatic assembly,[12,13] and hydrogen bonding.[20] These have little changed luminescence and defined QD loading amounts and ratios among differently sized QDs. Recently, Nie and co-workers reported that multicolor QDs have been successfully incorporated into multiporous latex or silica beads.[9−11] Also, small-sized smart hydrogels in response to pH or temperature were utilized to load differently sized QDs, creating multicolored nanospheres.[13,20] In addition to incorporation of QDs within the sphere interiors, engineering of the sphere surface also possessed multicolor optical shells, which can be fabricated by a layer-by-layer assembly technique[12] or a solvent-controlled precipitation.[21] However, the increasing understanding of the biological complexity leads to demands for further research at a cellular and molecular level. In this case, it seems that the development of multifunctional microstructures with imaging modes becomes of more importance. Nevertheless, a major problem is that no feasible design is currently available for integration of optical coding and other functions.

Even now, progress in functionalization of luminescent microspheres is made continuously. For example, an interesting derivative of QD bar codes may integrate magnetic nanoparticles in one single entity for magnetic resonance imaging (MRI).[22,23] Also, other related applications may be provided including targeted drug delivery, rapid biological separation, biosensors, and magnetic hyperthermia therapy.[24−26] Although the bifunctional magnetic/luminescent microspheres are intriguing and reported by some authors,[27−29] no report has detailed the development of the preparation of optical bar-coded microspheres with magnetic properties. This may be the first challenge. On the other hand, for bioapplications of multifunctional microspheres, the subsequent difficulty is that biomolecule probes such as oligonucleotides and antibodies can be effectively conjugated on the encoded microsphere surfaces. However, it is perhaps more important that such advances can be combined with multifunctional microspheres that contain specific molecules designed for molecular recognition, targeting compounds designed for homing in on sites, and imaging agents designed to light up.

Guided by these considerations, a feasible approach to preparation of luminescent/magnetic microspheres with cross-linked polymer shells is reported here. In the design of these multifunctional microspheres, we implemented the following criteria: (1) the presence of target species for homing in on the targeted site; (2) the involvement of imaging agents, aiming to image biological process; (3) incorporation of biomolecules or drugs into the microspheres by physical means; (4) a release mechanism induced by exterior stimuli such as a change in temperature. As a result, a structure was addressed in detail in which silica spheres with dotted Fe_3O_4 nanoparticles were coated by multicolor CdTe nanocrystals via metal ion-driven deposition, which was protected by formation of the outer silica shell. Then these luminescent/magnetic silica particles were used as seeds to grow a stimulus-responsive polymer shell. Stimulus-responsive polymers with specific functional groups can be regarded as ideal substitutes for the modification of the microsphere surface. In addition to the ability to conjugate proteins, particular cross-linking structures provide a means of protecting biomolecules, such as proteins, peptides, drugs, and oligonucleotides, from enzymatic in vivo degradation.[30] Herein, poly(*N*-isopropylacrylamide) (PNPAM), a well-known thermosensitive polymer, was chosen to add to the function of the microspheres. PNIPAM is water-soluble and hydrophilic below the lower critical solution temperature (LCST). Above this temperature, PNIPAM undergoes a sharp coil-to-globule transition to form inter- and intrachain association that results in an insoluble and hydrophobic aggregate. It has been demonstrated that its swelling/deswelling behavior in response to external temperature changes is favorable for nucleic acid adsorption, drug release, biomolecular conjugates, and so on.[31] Therefore, this may be a rational design of multifunctional microspheres for biomedical applications, especially in polymer-based circulating drug-delivery systems.

Experimental Section

Materials. $FeCl_3 \cdot H_2O$, $CdCl_2$ (99%), and thioglycolic acid (TGA) (98%) were purchased from Acros. Tellurium powder (99.8%) and NIPAM (97%) were obtained from Aldrich. $FeCl_2 \cdot 4H_2O$ and *N*,*N*′-methylenebisacrylamide (MBA) (98%) were purchased from Fluka. Trisodium citrate, potassium persulfate (KPS), sodium hydroxide (NaOH), $NaBH_4$, tetraethyl orthosilicate (TEOS), 3-(trimethoxysilyl)propyl methacrylate, (3-mercaptopropyl)trimethoxysilane, and aqueous ammonia solution (25 wt %) were analytical grade and commercially available products. All chemicals were used as received. The silica particles used were prepared via the modified Stöber route, and the diameter observed by TEM was ca. 100 nm.

(20) Gong, Y.; Gao, M.; Wang, D.; Möhwald, H. *Chem. Mater.* **2005**, *17*, 2648.
(21) Radtchenko, I. L.; Sukhorukov, G. B.; Gaponik, N.; Kornowski, A.; Rogach, A. L.; Möhwald, H. *Adv. Mater.* **2001**, *13*, 1684.
(22) Mulder, W. J. M.; Koole, R.; Brandwijk, R. J.; Storm, G.; Chin, P. T. K.; Strijkers, G. J.; de Mello Donega, C.; Nicolay, K.; Griffioen, A. W. *Nano Lett.* **2006**, *6*, 1.
(23) Tan, W. B.; Zhang, Y. *Adv. Mater.* **2005**, *17*, 2375.
(24) Wang, D.; He, J.; Rosenzweig, N.; Rosenzweig, Z. *Nano Lett.* **2004**, *4*, 409.
(25) Gaponik, N.; Radtchenko, I. L.; Sukhorukov, G. B.; Rogach, A. L. *Langmuir* **2004**, *20*, 1449.
(26) Yi, D. K.; Selvan, S. T.; Lee, S. S.; Papaefthymiou, G. C.; Kundaliya, D.; Ying, J. Y. *J. Am. Chem. Soc.* **2005**, *127*, 4990.
(27) Zebli, B.; Susha, A. S.; Sukhorukov, G. B.; Rogach, A. L.; Parak, W. J. *Langmuir* **2005**, *21*, 4262.
(28) Ma, D.; Guan, J.; Normadin, F.; Denommee, S.; Enright, G.; Veres, T.; Simard, B. *Chem. Mater.* **2006**, *18*, 1920.
(29) Lansalot, M.; Sabor, M.; Elaïssari, A.; Pichot, C. *Colloid Polym. Sci.* **2005**, *283*, 1267.
(30) Nayak, S.; Lyon, L. A. *Angew. Chem., Int. Ed.* **2005**, *44*, 1686.
(31) Gil, E. S.; Hudson, S. M. *Prog. Polym. Sci.* **2004**, *29*, 1173.

Preparation of Magnetite Nanoparticles. An iron oxide dispersion was prepared using the method already described,[32] based on the coprecipitation of $FeCl_2$ and $FeCl_3$ by adding a concentrated solution of base (10 M NaOH) onto the mixture of iron salts with a molar ratio ($FeCl_2$:$FeCl_3$) of 1:2. The alkaline solution was stirred for 1 h at 20 °C and then heated at 90 °C for 1 h. The ultrafine magnetic particles obtained were peptized by treatment with a nitric acid solution (2 M). The magnetite dispersion was then stirred for 30 min at 90 °C upon addition of a trisodium citrate solution (0.3 M). The excess citrate was removed by precipitation of magnetite nanoparticles with acetone. The magnetite dispersion was adjusted by 5 wt % for further use.

Preparation of Thiol-Capped CdTe Nanocrystals. The preparation of thioglycolic acid-capped CdTe nanocrystals has been described in detail by the hydrothermal route according to previous reports.[33] Briefly, fresh NaHTe solution was added to a N_2-saturated $CdCl_2$ solution in the presence of TGA at pH 9.0 in an ice−water bath. The ratio (i.e., [$CdCl_2$]:[TGA]:[NaHTe]) was fixed at 1:1.5:0.5 for all samples. Then the CdTe precursor solution (40 mL) was put into a Teflon-lined stainless steel autoclave with a volume of 50 mL. The autoclave was maintained at 180 °C for 50, 60, and 70 min for three size factions of CdTe nanocrystals with yellow, orange, and red emission color, respectively. Then it was cooled to room temperature by a hydrocooling process. In comparison with that of Rhodamine 6G at room temperature, the photoluminescence quantum yield (PL QY) of the preformed TGA-capped CdTe nanocrystals used in the text was estimated as 30−40%.

Synthesis of Silica-Coated Fe_3O_4@SiO_2@CdTe Particles. A suspension of the synthesized magnetic nanoparticles (0.1 g) was diluted by a mixture of ethanol (40 mL) and water (8 mL). After addition of ammonia solution (1 mL, 25 wt %), the precursor of TEOS (0.5 mL) was added to the reaction solution with mechanical stirring at 25 °C for 12 h. The preformed particles were washed to eliminate excess reactants by centrifugation and dispersed in an aqueous solution at 0.25 wt %.

The preformed CdTe nanocrystal was precipitated by ethanol, and powdered products made up the aqueous dispersion, which was adjusted for a proper absorbance value of 0.1−0.3 (at the maximum peaks). The molar concentration was calculated by the empirical formula according to the previous report.[34] The dispersions of CdTe (2 mL) and magnetic silica particles (2 g) were mixed, and then $CdCl_2$ aqueous solution in excess was added to the mixture at pH 7. The precipitates immediately appeared and were separated by the magnet. The washing procedure was necessary to completely remove the excessive Cd^{2+} in aqueous solution followed by drying the products.

The obtained powder had a poor dispersion in ethanol. When (3-mercaptopropyl)trimethoxysilane (2μL) was added, the solution became optically transparent and was stirred for 5 h. Then the outer silica shell was grown in the conditions of a mixture of water (5 mL) and ethanol (20 mL) containing TEOS (15 μL) as described elsewhere.[35]

Synthesis of PNIPAM-Coated Luminescent/Magnetic Microspheres. The obtained silica-coated luminescent/magnetic microspheres were further modified by adding 3-(trimethsilyl)propyl methacrylate (10 μL) for 12 h at 25 °C in the above water/ethanol mixture. The resulting products were collected via a magnetic field followed by washing with ethanol and water several times. In the polymerization procedure, an aqueous dispersion of the modified silica-coated luminescent/magnetic particles was used for the precipitation polymerization of NIPAM and the cross-linker MBA, using potassium sulfate (KPS) as an initiator. The reaction was allowed to proceed for 5 h at 70 °C. Finally, the products were washed using distilled water repeatedly and enriched with the help of a magnet.

Cell Culture. The CHO (Chinese hamster ovary) cells were obtained from the cell bank of Shanghai Science Academe. The cells were incubated in DMEM medium, containing calf serum (10%), penicillin (100 units/mL), streptomycin (100 μg/mL), and neomycin (100 μg/mL), in a fully humidified incubator at 37 °C with 5% CO_2.

When the cells reached 80% confluence with normal morphology, the PNIPAM-coated luminescent/magnetic microspheres were added to the cell dishes with a concentration of 500 μg/mL, and then these cell dishes were put into incubators for a desirable incubation time. Under such an incubation concentration, no detectable damage to the cells was observed. After incubation, these microsphere-loaded cells were washed with PBS three times to remove the unbound particles, and then the cell samples were readied for luminescence imaging measurements.

Characterization. Ultraviolet−visible (UV−vis) absorption spectra were measured on a Perkin-Elmer Lambda 35 UV−vis spectrophotometer. Fluorescence spectra were obtained at room temperature using an FLS920 spectrofluorimeter. If not specifically mentioned in the text, an excitation wavelength of 400 nm was used. X-ray photoelectron spectroscopy was performed on a PHI 5000C ESCA X spectrometer with Al Kα excitation (1686.6 eV). Transmission electron microscopy (TEM) images were obtained on a JEOL-1230 transmission electron microscope, and the samples for TEM measurements were obtained by placing one drop of the samples on copper grids coated with carbon. Scanning electron microscopy (SEM) was carried out on a Philips XL30 microscope, and the samples were loaded onto a glass surface previously sputter-coated with a homogeneous gold layer for charge dissipation during the SEM imaging. The hydrodynamic diameter of the particles was determined by quasi-elastic light scattering (Malvern Autosizer 4700). A vibrating-sample magnetometer (VSM) (EG&G Princeton Applied Research vibrating sample magnetometer, model 155) was used at 305 K to measure the magnetic moment. The ζ potentials of the silica particles were measured on a ζ potential analyzer (Brookhaven). The cellular images were acquired with a confocal laser scanning microscope (Olympus, FV-300, IX71).

Results and Discussion

Metal Ion-Driven Heterocoagulation of Thiol-Capped CdTe Nanocrystals with Silica Particles. Engineering of colloidal surfaces is a fashionable topic of applied chemistry in the field of developing new materials with tailored properties. The approach of layer-by-layer (LbL) alternate adsorption to prepare luminescent shells is a mature technique, which provides a defined shell composition on the colloidal core, with the shell thickness being a function of the number of deposited layers. However, the procedure is sufficiently time-consuming because it requires the removal of nonbound polyelectrolytes and nanocrystals at each step of the assembly. The presence of the polymer component in the nanocrystal-containing shells is also not always desirable. Radtchenko et al.[21] developed a modified route to formation of luminescent shells based on the solvent/non-solvent-pair technique or in aqueous solutions at different pH values.

(32) Sauzedde, F.; Elaïssari, A.; Pichot, C. *Colloid Polym. Sci.* **1999**, *277*, 846.
(33) Guo, J.; Yang, W.; Wang, C. *J. Phys. Chem. B* **2005**, *109*, 17467.
(34) Yu, W. W.; Qu, L.; Guo, W.; Peng, X. *Chem. Mater.* **2003**, *15*, 2855.
(35) Salgueiriˆno-Maceira, V.; Spasova, M.; Farle, M. *Adv. Funct. Mater.* **2005**, *15*, 1036.

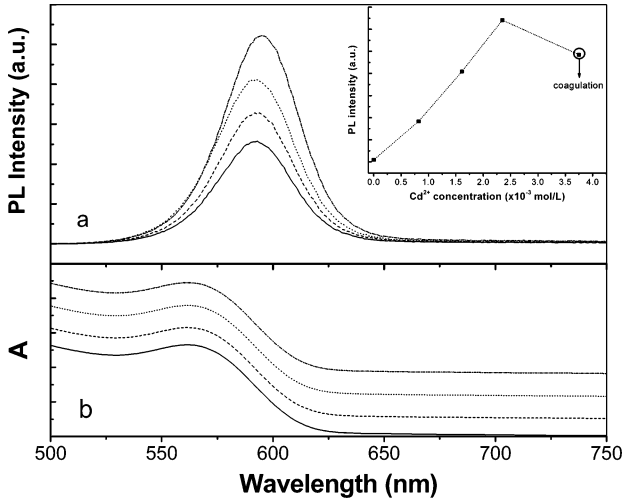

Figure 1. Fluorescence spectra (a) and UV−vis absorption spectra (b) of CdTe nanocrystals treated by adding different concentrations of Cd^{2+} solution. From bottom to top, the added concentration of Cd^{2+} is 0, 8.23×10^{-4}, 1.61×10^{-3}, and 2.35×10^{-3} mol/L, respectively. Inset of (a): PL intensity versus concentration of Cd^{2+}. The loop-marked dot means that CdTe nanocrystals were coagulated from aqueous solution after addition of Cd^{2+} solution (3.75×10^{-3} mol/L).

However, inorganic shells composed of thiol-capped CdTe with negative charges can easily be washed off when exposed to an aqueous solution or pH changes. A possible suggested reason is that a weak or lacking interaction between CdTe nanocrystals building up shells leads to diffusion of nanocrystals from the colloidal shells to aqueous solutions. As a result, a robust controlled precipitation must be developed to strengthen the luminescent shells in colloidal environments. The technique described herein, for the first time, allows the formation of robust luminescent shells based on metal ion (Cd^{2+})-driven coaggregation. This is a drastic acceleration in comparison to the multistep LbL approach that needs hours or even days to complete. Furthermore, the CdTe shells on colloidal cores remained intact in the aqueous solutions.

Luminescent CdTe nanocrystals stabilized by TGA, which were prepared via the hydrothermal route without posttreatment, possessed a negatively charged surface. Theoretically, by adding different concentrations of Cd^{2+} ion solution, it was possible to affect the dispersion stability of CdTe nanocrystals in aqueous solutions. A set of fluorescence spectra and UV−vis absorption spectra recorded under different concentrations of Cd^{2+} are shown in Figure 1. With an increase in the added concentration of Cd^{2+}, the fluorescence intensity was improved and the maximum was 2 times stronger than that of the original samples without addition of Cd^{2+}. However, from the inset of Figure 1a, after addition of more Cd^{2+} than before, coagulation of CdTe nanocrystals was clearly observed, leading to reduction of the detected fluorescence intensity. In Figure 1b, the addition of Cd^{2+} also results in an increase in the baseline. Due to the presence of CdTe aggregation upon addition of Cd^{2+}, the enhancement factor of the first electronic transition achieved should attribute to the light scattering or reflection originating from the aggregation particles. Furthermore, the stepwise increment of the baseline shows a tendency of aggregation of TGA-stabilized CdTe nanocrystals with an increase of the added amount of Cd^{2+}. Although a red shift of the fluorescence emission peak is observed in Figure 1a, the maximum absorption peak (561 nm) depending on the sizes of the QDs remains constant, indicating that added Cd^{2+} only influenced the surface properties of CdTe nanocrystals. It has been demonstrated that the lowly luminescent CdTe nanocrystals possess many more Te atoms at the surface than the highly luminescent ones.[36] Added Cd^{2+} may couple the surface Te atoms with dangling bonds and complex the residue-free TGA, forming thicker ligand shells. Such a surface results in a better confinement of photogenerated charge carriers, and thus, the effect would lead to higher photoluminescence intensity. The free Cd^{2+} may also be favorable for the coagulation of TGA-capped CdTe nanocrystals via the electrostatic interaction between COO^- ions of TGA and Cd^{2+}. When the nanocrystals come in close contact, the strong dipole−dipole interaction also leads to a red shift of the emission peaks.[37]

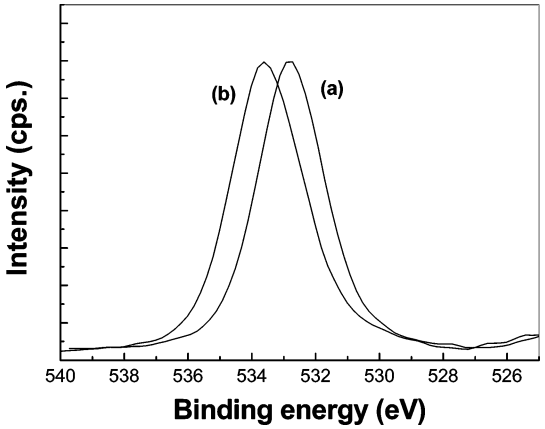

Figure 2. O 1s X-ray photoelectron spectral component of silica (a) and the product (b) treated by addition of Cd^{2+}.

To the best of our knowledge, among all investigations of the colloidal silica properties, the adsorption of metal cations (Zn^{2+}, Cu^{2+}, Cd^{2+}) has been a subject of wide interest. It has been shown that the adsorption of Cd^{2+} ions on silica increases strongly in the pH range 4−10.[38] As a result, via this specific property of the silica surface, it was possible that Cd^{2+} ions were used to build up the luminescent shells composed of TGA-capped CdTe nanocrystals on the silica. Also, some experiments related to the interaction between Cd^{2+} and hydroxide groups of the silica surface were conducted. Due to the higher charge density of the silica surface, compared with that of TGA-capped CdTe nanocrystals, when the added concentration of Cd^{2+} reached 1.61×10^{-3} mol/L, the coagulation of silica particles was observed. In Figure 2, it is shown that the nature of the silica particle surface changed before and after Cd^{2+} treatment using X-ray photoelectron spectroscopy (XPS). The spectra of the O 1s level were shifted by 0.8 eV to higher binding energy after addition of Cd^{2+}. This is consistent with the formation of alkoxide versus hydroxide oxygens, which demonstrates the presence of the adsorption of Cd^{2+} with the surface silanol.

(36) Borchert, H.; Talapin, D. V.; Gaponik, N.; McGinley, C.; Adam, S.; Lobo, A.; Möller, T.; Weller, H. *J. Phys. Chem. B* **2003**, *107*, 9662.
(37) Döllefeld, H.; Weller, H.; Eychmüller, A. *Nano Lett.* **2001**, *1*, 267.
(38) Prélot, B.; Janusz, W.; Thomas, F.; Villiéras, F.; Charmas, R.; Piasecki, W.; Rudzinski, W. *Appl. Surf. Sci.* **2002**, *196*, 322.

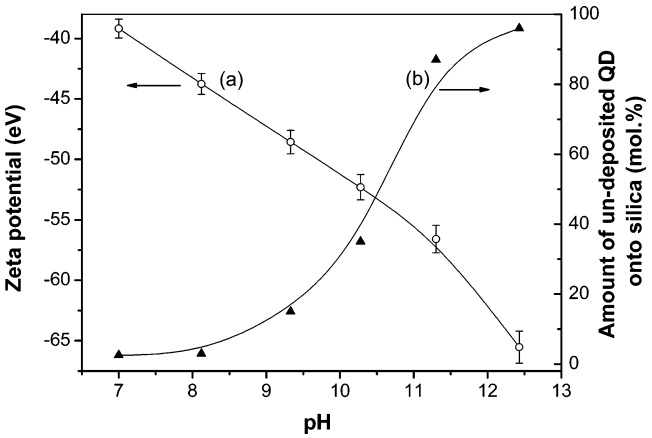

Figure 3. ζ potential of the silica particles (a) and the amount of undeposited CdTe nanocrystals on the silica particles (b) as a function of pH.

On the basis of the afore-conducted experiments, for controlling the morphology of composite particles, the important parameters must be considered including the concentration of the particles, the relative numbers of the component particles, and the contrast to their relative surface charges. In some cases, pH, temperature, and the nature of the ions will affect the products in the most sensitive way. In our system, owing to a decrease of the fluorescence intensity or even quenching of TGA-capped CdTe nanocrystals in the acid range, the deposition of QDs onto the silica particles was controlled in the pH range 7−12, and the other conditions (e.g., the particle number ratio $N_{silica}/N_{CdTe} = 1/800$ and the particle size ratio $D_{silica}/D_{CdTe} = 100/3$) remained constant. As shown in Figure 3a, it is reasonable that the ζ potential of the silica surface decreased with an increase of pH from 7 to 12.5, which originated from the transition of hydroxyl groups to alkoxides. In Figure 3b, it is observed that if the medium was controlled at pH 7−8, the amount of free QDs in the supernate after coprecipitation of silica particles and QDs was below 3% compared with the initial concentration of QDs (which was obtained by the ratio between $A_{residue}$ and $A_{initial}$ at the maximum peak). While pH was adjusted above 11, most of the QDs remained in the aqueous solution, which indicated the added Cd^{2+} cannot efficiently drive the heterocoagulation of two-component particles. The possible reason is that, at high pH, the added Cd^{2+} may correspond to the precipitation of hydrolyzed $Cd(OH)_2$ rather than to adsorption on silica particles or QDs.[38] Therefore, a stable system consisting of a regular composite particle could be prepared only in the medium controlled at pH 7−8.

Preparation of Silica-Coated Multi-Color-Encoded Fe_3O_4@SiO_2@CdTe Composite Microspheres. Iron oxide nanoparticles have been of great interest not only for the study of fundamental magnetic properties, but also for biomedical applications. Fe_3O_4, conjugated with various targeting molecules or antibodies, can be used to target specific cells in vitro. Some authors have reported a general strategy for the formation of solid-core/metal-nanoshell particles, using a combination of self-assembly of preformed nanoparticles onto larger spheres and colloid reduction chemistry.[35,39,40] In our system, Fe_3O_4 nanoparticles can be entrapped within SiO_2@CdTe composite microspheres in two different manners, i.e., dotted in the center of silica or covered on the surface of silica with CdTe nanocrystals. However, as considered theoretically regarding the latter, if both the magnetic nanoparticles and QDs were present on the colloidal surface simultaneously, a shift of the fluorescent emission peaks, a reduction of the quantum yields, and an extension of the excited-state lifetimes took place, being attributed to quenching interactions between the magnetic nanoparticles and QDs.[24] Hence, the heterocomposite nanoarchitecture, i.e., Fe_3O_4@SiO_2@CdTe microspheres, has been addressed in this study. The brief preparation procedure of these multifunctional microspheres was as follows: first, synthesizing the Fe_3O_4@SiO_2 particles (i.e., magnetic silica particles, MSPs) on the basis of the modified Stöber method and, second, loading a luminescent shell by Cd^{2+}-dirven coagulation of CdTe nanocrystals with MSPs. However, the noncovalent surface modification of nanoparticles has a serious limitation for biological applications, because the particles with small sizes may undergo biodegradation, and the exposed metal ion on the surface of nanoparticles can cause metal elemental toxicities in biological environments. Thus, the Fe_3O_4@SiO_2@CdTe microspheres could be designed to be covered with a homogeneous and smooth silica shell, avoiding corrosion of the CdTe shell. Moreover, the surface silanol groups can easily react with silane coupling agents to provide ideal anchorage for the covalent binding of specific ligands (streptadivin, antibodies, etc.).

Figure 4a shows TEM images of silica-coated Fe_3O_4 particles. Relying on the well-known Stöber method, the final MSPs with well-defined core/shell structures were rather monodisperse, even though silica shells have trapped more than one magnetic core. On the basis of the hydrolysis of TEOS, the thickness of the silica shell can be tuned from a few to several hundreds of nanometers by simply varying the initial amount of TEOS.[41] The Fe_3O_4@SiO_2 particles used in this case for the production of multifunctional microspheres had an average diameter of 100 ± 10 nm obtained by TEM images. Figure 4b is the TEM image of Fe_3O_4@SiO_2 particles densely loaded with TGA-capped CdTe nanocrystals. The preparation of heterocoagulates from the MSPs and QDs was first to mix the QDs and MSP dispersion with a fixed concentration ratio at optimal pH 7, followed by addition of Cd^{2+} to deposit the QDs onto the MSP surface. However, it was observed that the morphological nature of the CdTe nanocrystals might cause them to cluster and form islands at the MSP surface. This result is possibly due to different surface properties between CdTe nanocrystals and MSPs originating from the respective functional groups. Also, an added excess amount of CdTe nanocrystals may result in formation of clustered CdTe islands on the MSP surface. Figure 4c shows the TEM image of Fe_3O_4@SiO_2@CdTe particles covered with an outer silica shell. The principal idea of the formation of the outer silica shell is to avoid, or at least slow, the corrosion of QDs. Meanwhile,

(39) Stoeva, S. I.; Huo, F.; Lee, J. −S.; Mirkin, C. A. *J. Am. Chem. Soc.* **2005**, *127*, 15362.
(40) Sauzedde, F.; Elaïssari, A.; Pichot, C. *Colloid Polym. Sci.* **1999**, *277*, 1041.
(41) Deng, Y. H.; Wang, C. C.; Hu, J. H.; Yang, W. L.; Fu, S. K. *Colloids Surf., A* **2005**, *262*, 87.

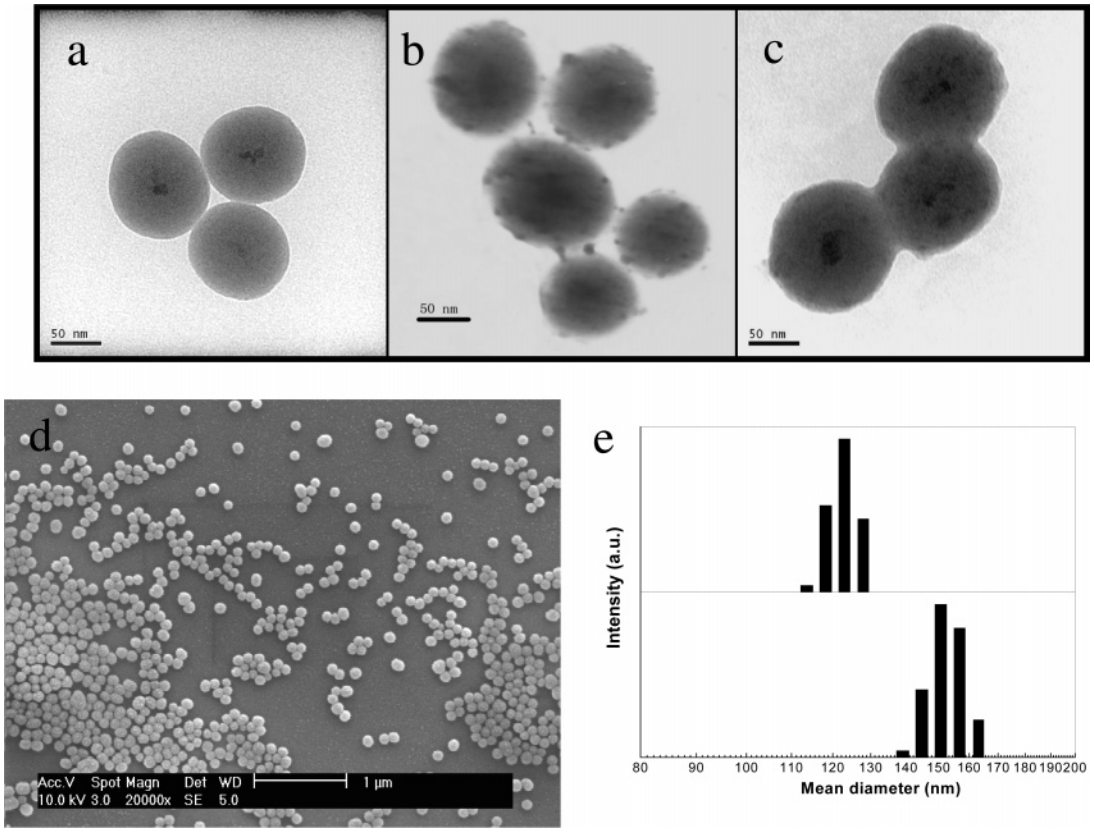

Figure 4. TEM images of (a) Fe_3O_4@SiO_2 particles, (b) Fe_3O_4@SiO_2@CdTe particles, and (c) Fe_3O_4@SiO_2@CdTe particles covered with an additional outer silica shell and the SEM image (d). The histogram (e) presents the hydrodynamic mean diameters for two sets of samples, i.e., top panel, Fe_3O_4@SiO_2 particles with an average diameter of 124 ± 15 nm, and bottom panel, silica-coated Fe_3O_4@SiO_2@CdTe microspheres with an average diameter of 158 ± 30 nm.

this was clearly shown for samples with an outer silica shell that kept a stable dispersion for a longer time compared to those without any protection. The total average increase in diameter was approximately 20 nm, and the samples still remained monodisperse, observed by the SEM image of Figure 4d. As shown in Figure 4e, it was also confirmed by dynamic light scattering (DLS) that the hydrodynamic diameters for the swollen silica-coated Fe_3O_4@SiO_2@CdTe microspheres increased by 34 nm in comparison with those of the Fe_3O_4@SiO_2 particles dispersed in aqueous solution.

The PL of the original CdTe dispersions was retained in the silica-coated luminescent/magnetic composite microspheres. The normalized PL emission spectra of the QDs and the silica-coated luminescent/magnetic composite microspheres are compared as shown in Figure 5. The maxima of the emission peak are red-shifted (around 5 nm in these cases) compared to those of the free QDs in aqueous solution after the CdTe shells on the surfaces of the magnetic silica particles are covered. Previous reports showed different results concerning the effect of silica coating on the luminescent properties of QDs. It has been demonstrated that the blue shift in the maximum of the emission spectra was due to the corrosion of QDs during silica deposition originating from the removal of their surface ligands.[42] However, in our cases, the slight red shift of PL emission peaks was due to the strong dipole−dipole interactions

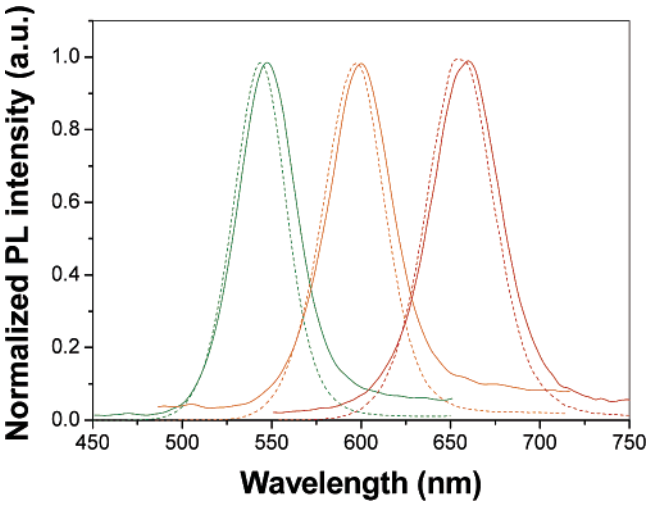

Figure 5. PL spectra of CdTe QDs (dotted line, 544, 597, and 655 nm) and silica-coated luminescent/magnetic composite microspheres (solid line, 547, 600, and 660 nm).

between the clustered QDs islanded on the surfaces of magnetic silica particles. In the silica covering route, (3-mercaptopropyl)trimethoxysilane (MPS) with TEOS was used to form the thin outer silica shell in the ethanol/water (4:1, v/v) solution. The exchange between MPS and TGA on the surfaces of QDs inhibited the presence of QDs entirely unprotected during silica growth, resulting in a few changes of the PL emission peaks.[19] However, when MPS passivated the surface of QDs, the capping was not perfect, leading to a decrease in the PL intensity as observed in these experiments. It should be noted, however, that the width of the

(42) Wang, Y.; Tang, Z.; Correa-Duarte, M. A.; Pastoriza-Santos, I.; Giersig, M.; Kotov, N. A.; Liz-Marzan, L. M. *J. Phys. Chem. B* **2004**, *108*, 15461.

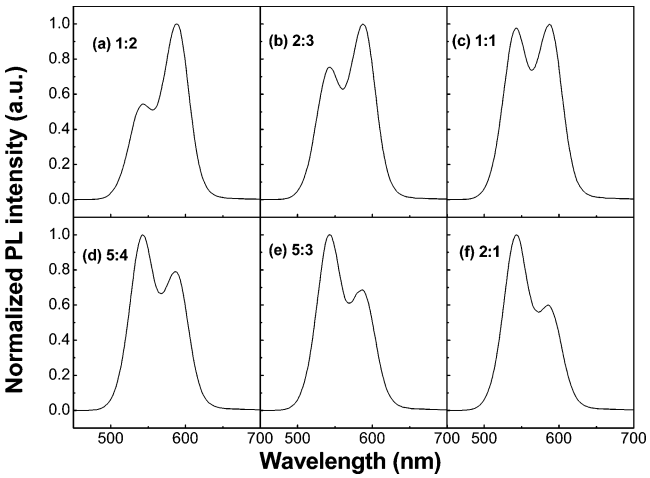

Figure 6. Photoluminescence spectra of two-colored QD-tagged microspheres showing two separate peaks (540 and 585 nm) with controlled intensity ratios (1:2, 2:3, 1:1, 5:4, 5:3, and 2:1).

emission peak of the QDs was not affected by the heterocoagulation and the outer silica shell covering.

In addition to single color-encoded microspheres, differently sized QDs can also be loaded onto the magnetic silica particles, which were rendered with distinguishable emission colors. Figure 6 shows the luminescence spectra taken from the aqueous dispersion of two-color tagged microspheres with six different ratios of the well-separated emission peaks. To the best of our knowledge, the ratios of the PL intensity can be tuned by two routes. One depends on the number of QDs trapped within the spheres. In the other way, the control of the relative emission intensity ratios can be allowed to create microspheres carrying unique multiplexed codes. As a result, according to the clustered CdTe shells with the improved PL intensity after addition of the Cd^{2+} solution, the latter way was adopted here. A certain amount of Cd^{2+} (2.35×10^{-3} mol/L) adjusted the luminescence intensity of two differently sized QDs. Then the heterocoagulates between MSP and CdTe were treated with Cd^{2+} in excess, followed by being covered with the outer silica shells. As shown in Figure 6, the intensity ratios of two emission peaks of silica-coated luminescent/magnetic microspheres were basically consistent with the designed original ratios. However, the precisely controlled ratio depending on the original adjustment of the PL intensity cannot be achieved after deposition of CdTe nanocrystals on the surfaces of MSPs. A possible reason is that the clustered CdTe nanocrystals with different sizes cause energy transfer, resulting in a slight deviation of the designed ratios.

Design of Surface Modification of Silica-Coated Luminescent/Magnetic Microspheres. The exploration of the interaction between nanostructured materials and living systems is of fundamental and practical interest. Inspired by this basic concept, we designed a rational model based on the hybrid nanomaterials of microgels and silica-coated luminescent/magnetic microspheres for drug delivery. Microgels have several important advantages over the others, including stability, ease of synthesis, good control over particle size, and easy functionalization providing stimulus-responsive behavior. In this demonstration, cross-linked PNIPAM covered the modified silica-coated luminescent/magnetic microspheres by precipitation polymerization, forming triple-layer/core nanostructures (i.e., cross-linked PNIPAM shell, thin silica layer-protected CdTe layer, silica layer, and Fe_3O_4 core from the outside to the inside). Recently, Lyon and co-workers[43] reported folic acid-labeled PNIPAM microgels that had potential to be used as carriers for cytosolic delivery of drugs to cells and exhibited temperature-dependent cytotoxicity. However, when cancer cells take up a large amount of nanomaterials containing folic acid to enable their rapid proliferation, the healthy cells may also phagocytize these microgels, leading to cell death induced by cytotoxicity of the loaded drugs or microgels by themselves. Furthermore, it is necessary determined whether the specific agents targeting cancer cells are of general usefulness. So far, physically driven forces to target tumors are the most effective. In our model, the design of coating Fe_3O_4 nanoparticles is inspired by this consideration. Meanwhile, it seems to be more important whether multifuctional microspheres without bound specific molecules can enter cells to be used as carriers for cytosolic drug delivery. In this case, the designed smart microstructures in our model provided CdTe layers with excellent imaging properties for possible use in this study.

On the basis of our previous work,[44] the cross-linked PNIPAM shell was synthesized by means of free radical precipitation polymerization following surface modification of silica-coated luminescent/magnetic microspheres with 3-(trimethoxysilyl)propyl methacrylate. Figure 7a shows the TEM images of PNIPAM-covered luminescent/magnetic microspheres with 10% cross-linking density (i.e., the weight percentage of *N*,*N*′-methylenebisacrylamide in the NIPAM monomers is 10%). As shown in the enlarged inset image, deswelling PNIPAM shells with a bright view were about 20 nm in thickness. The swelling/shrinking behavior of these microspheres with different cross-linking densities was measured by DLS as shown in Figure 7b. All the synthesized microspheres showed a narrow size distribution with a polydispersity index (PDI $= \langle \mu_2 \rangle / \Gamma^2$)[45] less than 0.082. As expected, the volume phase transitions took place continuously with increasing temperature except that microspheres with a lower cross-linking density of 5% displayed a sharper phase-transition curve than those for the samples with higher cross-linking densities of 10% and 15%. According to the DLS results, the swelling ratio of the microspheres (defined by $(D_{20°C}/D_{45°C})^3$, D = hydrodynamic diameter) decreased from 24.9 to 19.4 to 12.7 with increasing cross-linking densities from 5% to 10% to 15%. At the cell incubation temperature (37 °C), the average hydrodynamic diameter was ca. 165 nm for the three samples, which was a small enough size (below 200 nm) to maximize extravasation into the cells.[46] The swelling/deswelling behavior of these microspheres depending on the cross-linking density makes them very important as carriers in the fields of biology and medicine. As a result, an added amount of cross-linker

(43) Nayak, S.; Lee, H.; Chmielewski, J.; Lyon, A. L. *J. Am. Chem. Soc.* **2004**, *126*, 10258.
(44) Guo, J.; Yang, W.; Deng, Y.; Wang, C.; Fu, S. *Small* **2005**, *1*, 737.
(45) Chu, B, Wang, Z; Yu, J. *Macromolecules* **1991**, *24*, 6832.
(46) Das, M.; Mardyani, S.; Chan, W. C. W.; Kumacheva, E. *Adv. Mater.* **2006**, *18*, 80.

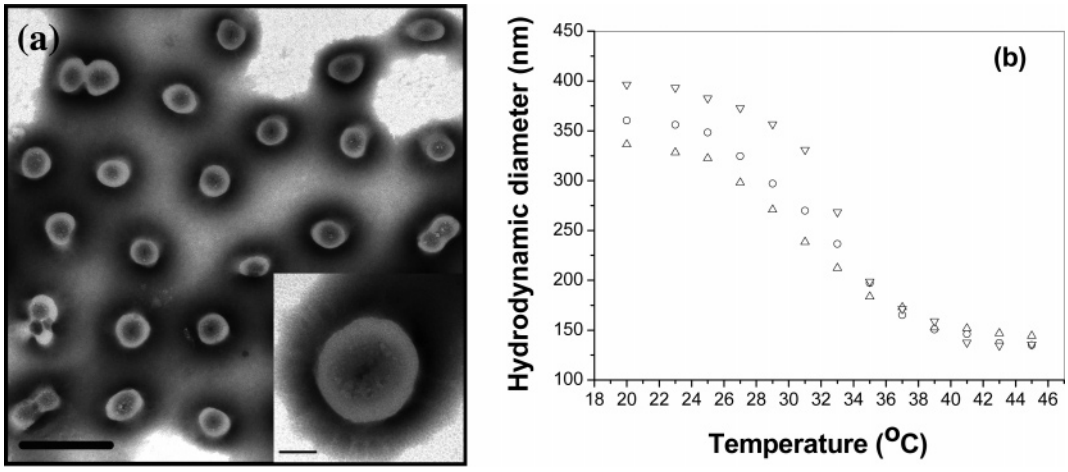

Figure 7. (a) TEM images of PNIPAM-covered luminescent/magnetic microspheres (scale bar 500 nm) and their enlarged view (inset, scale bar 50 nm). The background was stained with phosphate−tungstic acid. (b) Temperature dependence of the hydrodynamic diameter of PNIPAM-covered luminescent/magnetic microspheres with cross-linking densities of 5% (▽), 10% (○), and 15% (△).

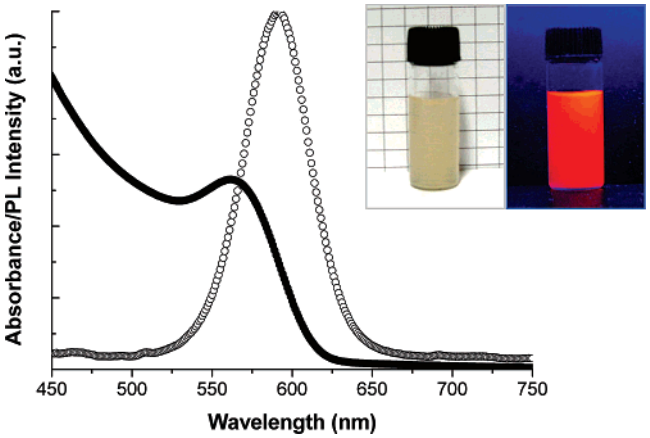

Figure 8. UV absorbance spectra (●) and photoluminescence spectra (○) of the PNIPAM-covered luminescent/magnetic microspheres dispersed in aqueous solution. Inset: photos taken in the sunlight (left) and under a 253 nm UV lamp (right).

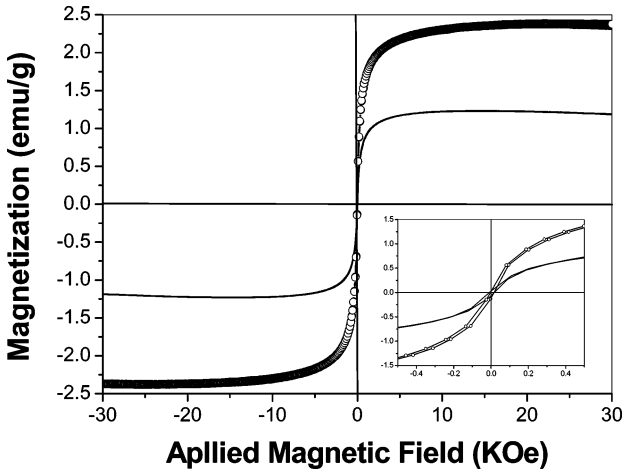

Figure 9. Magnetization curve of silica-coated Fe_3O_4@SiO_2@CdTe microspheres (○) and PNIPAM-covered luminescent/magnetic microspheres with a cross-linking density of 10% (solid line) at 305 K. The inset is a magnified view of the magnetization curves at low applied fields.

(MBA) should be taken into account for controlling the volume phase-transition temperature and swelling ratio of these multifunctional microspheres.

The PL properties of the microspheres were also characterized by UV−vis and fluorescence spectrometry as shown in Figure 8. It was observed that no significant change in the photoluminescence spectrum occurred after encapsulation of the cross-linked PNIPAM. This indirectly shows that the outer silica layers indeed protected the deposited CdTe layer from the corrosion of the different environments as well as being modified with silane agents. The photos in the inset in Figure 8 show the well-stabilized dispersion with coupling of cross-linked PNIPAM shells even stored after several weeks, which retains the strong PL intensity.

Magnetic measurements of silica-coated Fe_3O_4@SiO_2@CdTe particles and PNIPAM-covered luminescent/magnetic microspheres were carried out using a vibrating-sample magnetometer. As shown in Figure 9, the saturation magnetic moments of silica-coated Fe_3O_4@SiO_2@CdTe particles and PNIPAM-covered luminescent/magnetic microspheres reached 2.35 and 1.16 emu/g, respectively. These low saturation magnetization values were less than the reference value for the pure magnetite nanoparticles (64.3 emu/g). This can be explained by considering the diamagnetic contribution of the silica shells surrounding the magnetite nanoparticles, which also weakened the magnetic moment for PNIPAM-covered luminescent/magnetic microspheres due to the presence of thicker shells. In addition, both of them showed a superparamagnetic property at 305 K indicated by the inset figure, which exhibited no remanence effect from the hysteresis loops at low applied magnetic field. These magnetic properties are critical in the applications of the biomedical and bioengineering fields. When the microspheres undergo strong magnetization, the efficient magnetic separation is allowed for, and when the applied magnetic field is removed, redispersion of these microspheres will take place rapidly.

In this study, CHO cells were chosen to investigate the cellular uptake of the PNIPAM-covered luminescent/magnetic microspheres. When the cells were excited with a 488 nm laser beam in a confocal microscope, the fluorescent views of cellular marker microspheres were recorded as well as the differential interference contract (DIC) images acquired simultaneously in a transmission channel to exhibit the cell morphology as shown in Figure 10. Figure 10a shows the intracellular distribution of luminescent microspheres in the representative CHO cells, where the main image demonstrates the cellular markers in the $x-y$ plane and both the

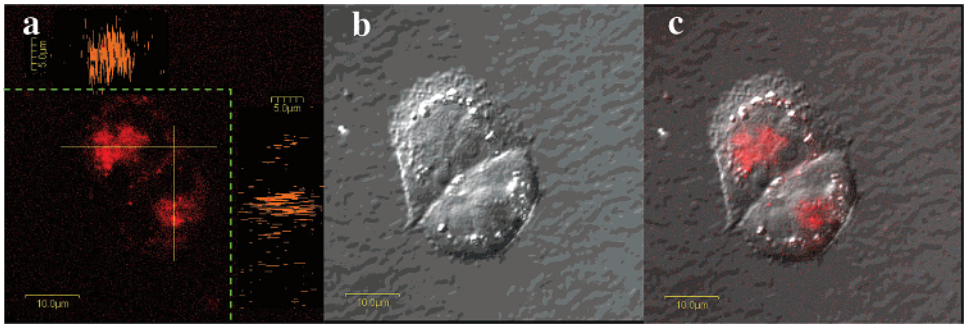

Figure 10. Confocal images of representative CHO cells from the cells incubated in the presence of PNIPAM-covered luminescent/magnetic microspheres: (a) photoluminescence image of cellular marker microspheres in the $x-y$ (main part), $y-z$ (right panel), and $x-z$ (top panel) planes, (b) DIC image of the CHO cells, (c) overlap of both the images of (a) and (b).

top and right panels exhibit the microsphere distributions in the $x-z$ and $y-z$ planes along the marked lines in the main image obtained by z-scanning, respectively. The luminescent microspheres were found to mainly distribute in the cytoplasm of the cell, which is consistent with the folic acid-conjugated PNIPAM microgels or an analogous system.[43,47] However, in Figure 10a, several light spots in the main image are clearly observed other than the aforementioned uniform distribution of cellular QDs,[48] which suggests the presence of aggregates of microspheres inside the cells. This may show that, above the LCST, PNIPAM microspheres with a bigger size (>100 nm) in cell media can cause more protein adsorption and denaturation, which lead to significant aggregation of microspheres in the cytosol. Small-sized particles such as micelles or deswellon hydrogels apparently retained the stability of the dispersion or thermosensitive property according to previous reports.[43,47] In spite of the presence of intracellular aggregation and protein adsorption on the microspheres, it should be noted that luminescent/magnetic microspheres with hydrophobic PNIPAM shells above the LCST can be taken up by the cells. This suggests that an unknown endocytosis mechanism may have worked in this case, different from the receptor-mediated endocytosis process. Further work is required to look for other effects on the cell physiology based on our model, which is our subsequent focus. In this study, these structures still have potential to be used as carriers for cytosolic delivery of drugs to targeted cells, which show the possibility of (i) uptake with cells, (ii) subcellular distribution in the cytosol, (iii) fluorescence tracing determination, and (iv) magnetic targeting using exterior magnetic fields.

Conclusion

In summary, we presented a rational design to prepare luminescent/magnetic composite microspheres with combined advances for biomedical applications. Here, the aggregation of thiol-capped CdTe on silica particles was induced, for the first time, by the metal ion (Cd^{2+}) coprecipitation technique, leading to formation of a luminescent shell with multicolor bar codes, as is the case in the LbL approach. However, this method has other significant advantages, which are the reduced time of the procedure and the possibility to create functional shells in only one step. Before the coagulation between silica and CdTe nanocrystals, magnetite nanoparticles were also dotted in the center of the silica spheres using the well-known Stöber method, addressable by a magnetic field. The obtained Fe_3O_4@SiO_2@CdTe particles were coated by an outer shell of silica for avoiding the corrosion of CdTe shells, while providing a robust platform for the covalent binding of specific ligands. The luminescent/magnetic composite microspheres maintained the intense spectral signatures and the photostability, allowing for the real-time study of long-lived biological processes. Induced by this, the composite microspheres were used as seeds to cover the cross-linked PNIPAM shells responding to phase transition of the exterior temperature, creating multifunctional microspheres in the submicrometer size range. For intracellular drug delivery, we demonstrated that PNIPAM-covered luminescent/magnetic microspheres were also able to be taken up by CHO cells without inducement of any specific ligands. Different from the receptor-mediated endocytosis, this process may be related to the interactions of cells and shrinking PNIPAM shells with hydrophobic properties at the cell incubation temperature (37 °C), but the exact reason is still unknown. Also, this is a current focus of our efforts. The designed multifunctional microspheres have much promise in detecting and treating cancer at its earliest stages due to their advances of magnetic targeting, excellent imaging, and drug-carried matrices and will be extended to in vivo systems in the next experiments.

Acknowledgment. This work was supported by the National Science Foundation of China (Grants 20374012 and 50403011), the National Science Foundation for Distinguished Young Scholars of China (Grant 50525310), the Shanghai Rising-Star Program (Grant 05QMX1404), and STCSM.

CM060976W

(47) Savic, R.; Luo, L.; Eisenberg, A.; Maysinger, D. *Science* **2003**, *300*, 615.
(48) Ma, J.; Chen, J. Y.; Guo, J.; Wang, C. C.; Yang, W. L.; Xu, L.; Wang, P. N. *Nanotechnology* **2006**, *17*, 2083.